OPEN

Spectroscopy of single Pr^{3+} ion in LaF_3 crystal at 1.5 K

Ippei Nakamura, Tatsuya Yoshihiro, Hironori Inagawa, Satoru Fujiyoshi & Michio Matsushita

Department of Physics, Tokyo Institute of Technology, Ookayama 2-12-1 Meguro Tokyo, 152-8550 Japan.

Optical read-out and manipulation of the nuclear spin state of single rare-earth ions doped in a crystal enable the large-scale storage and the transport of quantum information. Here, we report the photo-luminescence excitation spectroscopy results of single Pr^{3+} ions in a bulk crystal of LaF_3 at 1.5 K. In a bulk sample, the signal from a single ion at the focus is often hidden under the background signal originating from numerous out-of-focus ions in the entire sample. To combine with a homemade cryogenic confocal microscope, we developed a reflecting objective that works in superfluid helium with a numerical aperture of 0.99, which increases the signal by increasing the solid angle of collection to 1.16π and reduces the background by decreasing the focal volume. The photo-luminescence excitation spectrum of single Pr^{3+} was measured at a wing of the spectral line of the $^3H_4 \rightarrow {}^3P_0$ transition at 627.33 THz (477.89 nm). The spectrum of individual Pr^{3+} ions appears on top of the background of 60 cps as isolated peaks with intensities of 20–30 cps and full-width at half-maximum widths of approximately 3 MHz at an excitation intensity of 80 $W\,cm^{-2}$.

In the solid state, if individual spins of nuclei or electrons are optically read-out and manipulated, the system would become attractive in quantum information technology because the transport and processing of quantum information are directly coupled with photons. In this context, extensive studies have been conducted on systems such as defect centers in diamonds[1,2], quantum dots[3], and impurity atoms in semiconductors[4]. The nuclear spin of rare-earth (RE) ions doped in an inorganic crystal is also a suitable system for quantum-information processing[5]. At a temperature of a few K, the homogeneous width of the optical transition of a RE ion between $4f$ states narrows to almost a lifetime-limited width at approximately 10 kHz, whereas the inhomogeneous width caused by the crystal field is 5–7 orders of magnitude larger[6]. This difference allows us to address ions individually using their transition frequencies, even if the ions are at a distance within the diffraction limit.

The basis of the optical detection and manipulation of RE spins has been studied for an ensemble of spins[7–9], and pioneering works[10–15] for individual RE ions are pushing the frontier forward. However, only a few experiments have been successful in resolving the nuclear spin states of single RE ion in a solid[13,14]. As an inevitable result of the narrow homogeneous width, optical detection of single RE ions is hampered by weak spontaneous emission of the ions. In addition, even with the confocal configuration, in which the excitation focus coincides with the detection focus, emission from the entire crystal adds up in the background and deteriorates the signal-to-background ratio. One of the methods to circumvent the weak emission of the ion is to convert photo-emission into a different photo-physical event for easier detection, for example, detecting up-conversion luminescence from the $5d$ state of the RE ion at room temperature[16] or detecting photo-ionization of a single RE ion using a single electron transistor[13]. The background problem can be overcome with the use of a nanocrystal sample[10–12,14,16]. In the measurement of single Pr^{3+} in a nanocrystal of Y_2SiO_5, the nanocrystal was placed on a solid immersion lens to improve the photon-collection efficiency[14].

Our approach is to develop a high numerical aperture (NA) objective that works at a few K. A larger solid-angle of collection and a smaller focal volume of the new objective makes our setup sensitive enough to detect a single Pr^{3+} ion in a bulk crystal. In application to nuclear spin qubit, qubit manipulation is conducted under a static magnetic field to use Zeeman sublevels. Because the Zeeman effect is anisotropic, the magnetic field must be applied along a well-controlled direction with respect to the host crystal. If optical detection of a single ion is established for a bulk crystal, optical access to a single ion under the Zeeman field will be readily attained.

Results

Figure 1 shows the essential part of the setup including the new objective. To keep the point emitter at the focus and continue a stable measurement for several hours, the sample and the objective must be mounted on a single-component holder in superfluid helium[17]. Because there are no commercially available objective works in
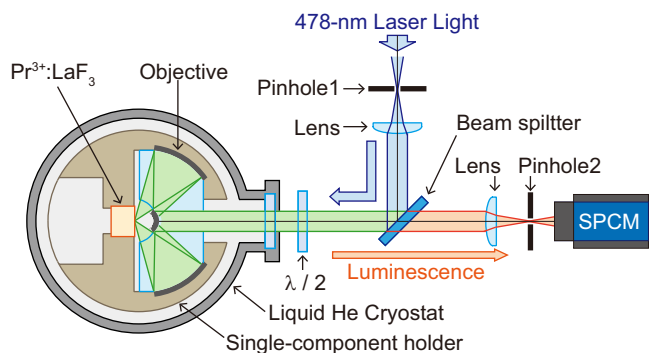
Figure 1 | Schematic representation of our homemade confocal setup for detecting a single Pr^{3+} ion doped in LaF_3 at 1.5 K. The reflecting objective focuses the incident beam and collects the emission from the sample with its aspheric convex mirror and spherical concave mirror. A single-mode fiber serves as pinhole 1, and a multi-mode fiber serves as pinhole 2 for the real setup. The half wave plate ($\lambda/2$) was used to rotate the linear polarization angle of the laser. SPCM is the single photon counting module. See Methods for further details of the confocal setup and the light source.

Figure 2 | Electronic states and hyperfine structure of Pr^{3+}:LaF_3. The nine-fold degeneracy of the ground $^3H_4$ state is lifted in LaF_3 by the crystal field of C_2 symmetry. Both the ground $^3H_4$ and the excited $^3P_0$ states split into three sublevels to show the hyperfine structure due to Pr nuclear spin ($I = 5/2$). For the $^3H_4$ state, the energies of the three hyperfine sublevels with respect to the lowest are 0, 16.7, and 25.2 MHz. For the $^3P_0$ state, only the two adjacent splittings are known to be 0.7 and 1.1 MHz.

superfluid helium, we developed a single-component reflecting objective consisting of two mirrors[18,19]. Robust optical alignment of the objective at a few K is guaranteed by fabricating two mirrors on a single piece of fused silica; the reflecting design eliminates chromatic aberration. In the new objective designed in the present work, one of the two mirrors was made aspherical. Therefore, NA reached 0.99 (see Methods), almost the maximal NA in superfluid helium, i.e., n_{He} sin(90°) = 1.03, where n_{He} is the refractive index of superfluid helium[20]. The design and performance of the new objective will be described in detail in another publication by our group (Inagawa, *et al.* manuscript in preparation).

Photo-luminescence excitation spectra were measured at 1.5 K for a Pr^{3+} doped LaF_3 (Pr^{3+}:LaF_3) crystal using the homemade reflecting confocal microscope. Pr^{3+} ions substitute 0.05% of La^{3+} ions in the crystal. The size of the crystal is $4 \times 5 \times 6$ mm³. Figure 2 shows the electronic ground and excited states and their hyperfine structure[21–23]. Both the ground $^3H_4$ and excited $^3P_0$ states split into three hyperfine sublevels due to the Pr nuclear spin ($I = 5/2$). No matter to which hyperfine sublevel the Pr^{3+} ions are excited, the excited ions relax to all the three ground-state sublevels. Therefore, excitation by a single-frequency laser causes population transfer of the Pr nuclear spin to non-resonant sublevels (so-called the optical pumping effect). The ions stop luminescence until the nuclear spin relaxes back to the resonant hyperfine sublevel, which occurs with a time constant longer than 1 s[24]. In all the experiments described below, an acousto-optic modulator (AOM) was used as a laser-frequency multiplexer to avoid this quenching. The laser diffracted by the AOM had three frequency components at 0, 8.5, and 25.2 MHz with respect to the lowest component (see Methods). The excitation with the three frequencies made all the three $^3H_4$ hyperfine sublevels simultaneously resonant with transitions to one hyperfine sublevel of $^3P_0$.

Figure 3a shows the photo-luminescence spectrum of 0.05% Pr^{3+}:LaF_3 taken at 1.5 K. The $^3H_4 \rightarrow {}^3P_0$ transition appeared at $\nu_0 = 627.33$ THz ($\lambda_0 = 477.89$ nm) with a full-width at half-maximum (FWHM) linewidth of 13 GHz. Figures 3b–g present the photo-luminescence excitation spectra of the Pr^{3+} ions in a confocal volume taken at different frequency positions in the inhomogeneously broadened spectrum of the ensemble of ions shown in Fig. 3a. When the excitation spectrum was measured, at frequencies further from ν_0, less resonant ions were in the focus. At a certain frequency, the number of the ions becomes so small that the spectral peaks of individual ions will be observed isolated from each other[25]. The maximum luminescence signal intensity can be estimated as follows.
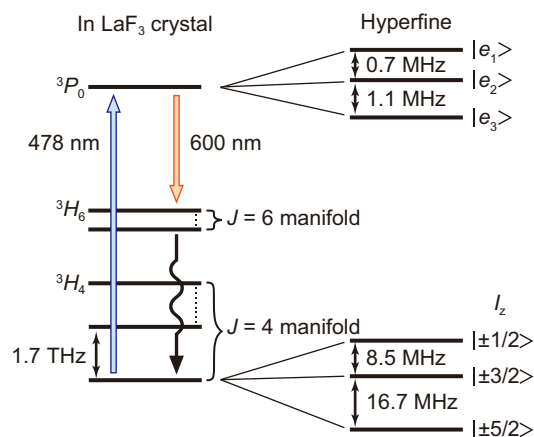
From the spontaneous emission rate of the $^3P_0$ state ($1/T_1 = 2.1 \times 10^4$ s^{-1}) and the luminescence quantum yield of the $^3P_0$ state (0.63)[26], the maximum number of luminescence photons emitted from a single Pr^{3+} is calculated to be 1.3×10^4 s^{-1}. Among the radiative deactivation processes from $^3P_0$, the probability of emission at a wavelength longer than 530 nm, which is the cut-off wavelength of a long-wavelength-pass filter, is calculated from ref. 27 to be 0.52. Upon further consideration of the detection efficiency of the setup (0.43%, for details, see Methods), the maximum photon signal from a single Pr^{3+} (I_{single}) is estimated to be 30 cps. In the measurement shown in Figs. 3b–g, a scan of 40 MHz was performed by acquiring photon counts every 0.2 MHz using the single-photon counting module (SPCM). Usually, the photon counts were accumulated for 1 or 2 s, and this scan was repeated 8 or 4 times, respectively, such that the total accumulation time per data point was 8 s. The average of the repeated scans is displayed in the figure. The focus of the setup was adjusted to the surface of the LaF_3 crystal using surface reflection. The total excitation intensity of the three frequency components was approximately 80 W cm^{-2}.

At $+0.04$ THz from ν_0 (Fig. 3b), the average of the signal is approximately 330 cps, and within a 40 MHz scan, the signal varies in intensity between 300 and 360 cps. At $+0.09$ THz from ν_0 (Figs. 3c and d), the average and variation of the signal decrease to approximately 90 cps and between 70 and 105 cps, respectively. Figures 3c and d were taken at different spatial positions on the crystal surface. At some spatial positions, structures narrower than 5 MHz can be observed. At $+0.10$ THz from ν_0 (Figs. 3e and f), the signal further decreases to an average between 60 and 90 cps. Figures. 3e and f were taken at different spatial positions at the crystal surface. On top of the frequency-independent flat signal at the average intensity, a couple of peaks with heights of approximately 20 cps and FWHMs of approximately 3 MHz appear. For the flat part of Fig. 3f between -5 and $+15$ MHz, the average signal intensity is 90.7 cps, and the standard deviation (sdev) is 4.3 cps. The deviation from the average can be explained as Poisson noise of the flat signal and that of the dark count of the detector of 12.3 cps, which was subtracted before, as observed in the figure. Note that the photon-count accumulation time was 8 s. Apart from the contribution from the flat signal and the dark count, the spectrum consists of only a couple of isolated peaks of 15–25 cps. At $+0.14$ THz from ν_0 (Fig. 3g), the signal decreases further to approximately 40 cps and
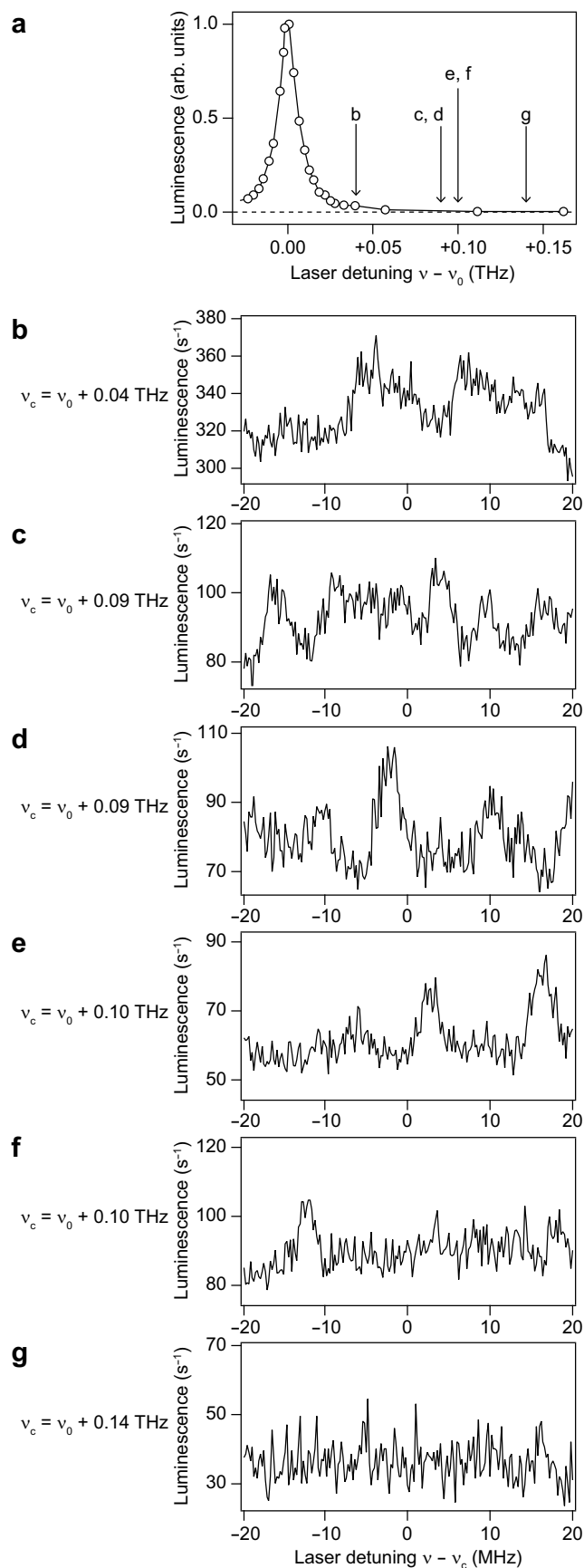
Figure 3 | **Photo-luminescence excitation spectrum of 0.05% Pr^{3+}:LaF_3 at 1.5 K.** (a) The inhomogeneously broadened spectrum of the $^3H_4 \rightarrow {}^3P_0$ transition. The horizontal axis represents the laser frequency as detuning from $\nu_0 = 627.33$ THz (477.89 nm), the center of the inhomogeneous

broadening. The width of the spectrum is 13 GHz in FWHM. (b–g) High resolution spectra acquired at various frequency positions in the inhomogeneously broadened profile of the ensemble displayed in (a). The horizontal axis represents the laser frequency scanned by AOMs, and ν_c is the center of the scanning range. The vertical axis represents the photon number detected by the SPCM. The dark count of the SPCM was subtracted before the figure was created. The total intensity of the three frequency components was 75–79 W cm^{-2}.

is almost completely flat without peaks with the size observed in Figs. 3e and 3f. Two peaks appeared in Fig. 3e at +2.8 and +16.4 MHz are probably signals of individual Pr^{3+} ions. There are some other experimental results which support the interpretation of the peaks as signal from single ions.

Figure 4 shows the spatial dependence of the excitation spectrum. The upper curve presents the spectrum of Fig. 3e, which contains a couple of peaks on a flat signal. The lower curve presents the spectrum taken at a different lateral position in the focal plane. The focus of the objective was displaced 0.29 μm horizontally and 0.61 μm vertically from the position at which the upper curve was measured. The two peaks in the upper curve at +2.8 and +16.4 MHz disappear in the lower curve. The lateral size of the focus of the objective was evaluated at 532 nm to be 0.21 μm (see Methods). Because the two peaks disappear when the focus moves more than its size, luminescence yielding the two peaks emanates from the focus of the objective. By contrast, because the flat signal does not change when the focus moves, the flat signal originates from the out-of-focus volume of the bulk sample.

Figure 5 shows the effect of excitation by three frequency components. The two spectra in the figure were acquired at the same spatial position in the crystal as the spectrum of Fig. 3e. The three frequency components were 0, 8.5, and 25.2 MHz when recording the black spectrum and 0, 16.7, and 25.2 MHz when recording the blue spectrum. The two peaks at +2.8 and +16.4 MHz are present only in the black spectrum, not in the blue spectrum. In recording the black spectrum, all three ground-state hyperfine sublevels are in resonance with the excitation light, whereas in recording the blue spectrum, only two of the three sublevels are in resonance, such that the nuclear spin population is transferred to the non-resonant sublevel by the optical
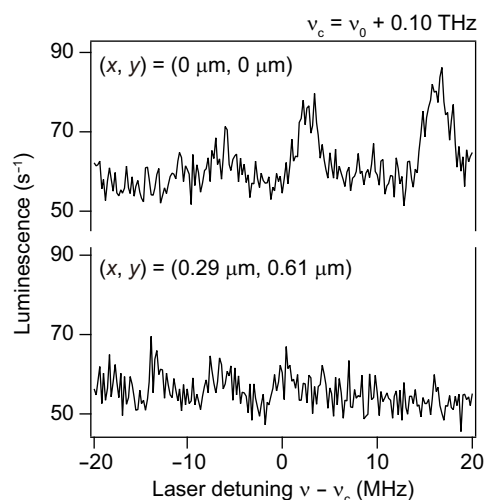

Figure 4 | **Spatial dependence of the excitation spectrum.** The upper curve shows the same spectrum as that presented in Fig. 3e. The lower curve is the spectrum taken at a different location on the crystal surface from that that used for the upper curve but using the same frequency range. The objective focus was displaced 0.29 μm horizontally and 0.61 μm vertically on the surface of the sample.
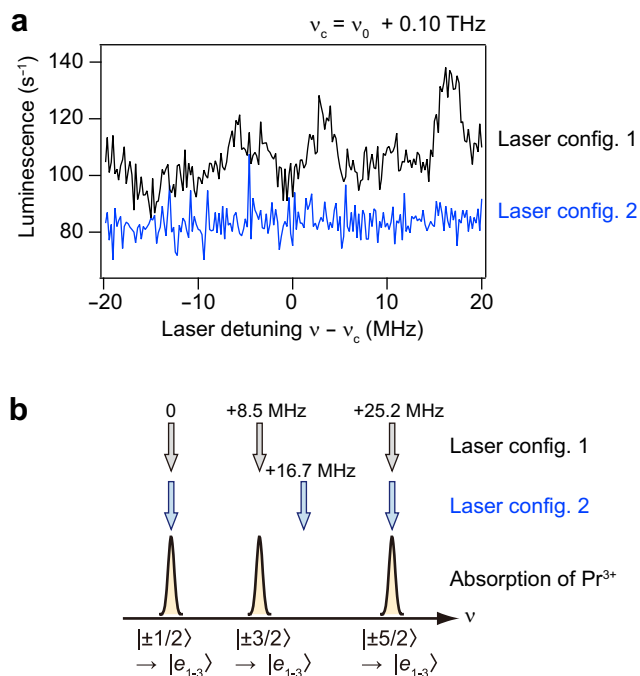
Figure 5 | Quenching of a photo-luminescence excitation spectrum due to optical pumping of Pr nuclear spin. (a) Photo-luminescence excitation spectra of the same frequency range as the spectrum of Fig. 3e with a total intensity of 157 W cm^{-2}. The laser configuration of the three frequencies was (0, +8.5, +25.2 MHz, config. 1) for the black curve and (0, +16.7, +25.2 MHz, config. 2) for the blue curve. (b) Schematic of the two frequency configurations of the excitation light (black and blue arrows) and the absorption spectrum of a single Pr^{3+} ion from the three hyperfine sublevels of the ground $^3H_4$ state.

pumping, and the resonant sublevels become empty. In the blue spectrum, the flat signal does not completely vanish because many of ions residing in the out-of-focus volume are not subjected to the optical pumping effect due to weak excitation by the out-of-focus light.

Figure 6 shows the saturation and the polarization measurement of the photo-luminescence excitation spectrum. Figure 6a is the spectrum acquired at +0.08 THz from ν_0. The excitation power dependence was measured for the peak at -3.8 MHz. The luminescence intensity was determined by Gaussian fitting of the excitation spectrum at several different excitation intensities and plotted in Fig. 6b. The solid curve is the saturation curve calculated as the steady-state population of the excited state on the assumption that all three ground-state sublevels are in resonance with the excitation light to one of the excited-state sublevels. The power dependence is expressed as $I(W) = I_{max} W/(W + W_{sat}/2)$, where W is the total excitation intensity. The two parameters, the maximum luminescence intensity I_{max} and the saturation excitation intensity W_{sat}, were determined by fitting to be 45 ± 5 cps and 219 ± 43 W/cm^{-2}, respectively. The maximum intensity of 45 cps is consistent with the estimation of $I_{single} = 30$ cps from the parameters of the bulk measurements. Figure 6c shows polarization dependence of the peak at -3.8 MHz in Fig. 6a. The luminescence intensity of the peak at -3.8 MHz exhibited a sinusoidal dependence of $\sin 2\theta$, where θ is the polarization angle of the linearly polarized excitation light, while that at -9.0 MHz did not exhibit particular variance. In the present experiment, the laser light propagates parallel to the crystalline c-axis, which has 3-fold symmetry. The Pr^{3+} site symmetry is C_2, and the $^3H_4 \rightarrow {}^3P_0$ transition dipole is along the C_2 axis[28]. Because there are three different C_2 axes in the plane perpendicular to the c-axis, numerous Pr^{3+} ions occupy three different oriented C_2 cites randomly, and in this case, the polarization dependences of the Pr^{3+}

ions cancel each other as observed in the measurement of the ensemble of Pr^{3+} ions at the center frequency ν_0 (Fig. 6d). Only a single ion and very few ions that are aligned parallel by accident exhibit the deepest modulation to the minimum value of zero.

The experimental results examined so far support that the 3 MHz-wide peaks of 20 cps, like those recorded in Fig. 3e, originate from single Pr^{3+} ions. These peaks were spectrally resolved from the signal of other Pr^{3+} ions contained in the focal volume of the NA = 0.99 objective at the wing of the inhomogeneously broadened spectrum (Figs. 3b–g) Emitters yielding these isolated peaks were confirmed to be spatially localized within the focus by moving the focus more than its size (Fig. 4). Depending upon the position of the focus, from zero to a few peaks are found in the same frequency region. The peaks appeared only when the excitation laser is in resonance with the transitions of all the three hyperfine sublevels of the ground state (Fig. 5). This result confirms that the peaks are the signals of Pr^{3+} ion and demonstrates optical control of Pr nuclear spin through optical pumping. The maximum luminescence intensity I_{max} derived from the power-dependence measurement (Fig. 6b) is consistent with the estimation based on the known parameters of the bulk. The polarization dependence (Figs. 6c and 6d) is the same as that expected for a single emitter.

Discussion

The photo-luminescence excitation spectrum of single Pr^{3+} measured in the present study does not exhibit excited-state hyperfine splitting of 0.7 and 1.1 MHz[22]. The laser carrying three frequency components causes all the three ground-state hyperfine sublevels to be in resonance with the transition to one of the excited-state sublevels. Therefore, the excitation spectrum does not show hyperfine splitting of the ground state but should reflect that of the excited state.

In the hole-burning experiment using the same setup as the single Pr^{3+} experiment, the hole width of 0.4 MHz at low power limit was broadened to 0.8 MHz at the excitation intensity of 40 W cm^{-2}. The photo-luminescence excitation spectra in Figs. 3–5 were measured with at least 75 W cm^{-2} of excitation intensity. The excitation spectra taken at this power level are considered to be subjected to power broadening to some extent. Other possible mechanisms that cause broadening of the excitation spectrum are spectral diffusion occurring at the interface of the crystal and superfluid helium, magnetic interaction with surrounding nuclei, and permanent electric dipole interaction with surrounding Pr^{3+} ions. To investigate the interaction with the surroundings that causes broadening of the single Pr^{3+} spectrum, the excitation intensity must be kept low enough to suppress power broadening. The weakest excitation employed in the present study was 15 W cm^{-2}, and the luminescence signal was only 6 cps. The detection efficiency of the present experiment was too poor.

The detection efficiency can be improved by combining the newly developed objective with a solid immersion lens[2,15] or planar dielectric antenna[29]. The solid angle of collection is 1.16π, where the solid angle that the inner convex mirror spans is subtracted from the solid angle that the larger concave mirror spans (see Methods). When the sample is inside the host crystal, the solid angle of collection is reduced to 0.30π. If the effect of refraction was absent, the solid angle of collection is 4 times larger and the volume of the focus will be smaller by a factor of $(n_{He}/n_{LaF3})^3 = 0.3$.

In summary, using a newly developed high-NA objective that works in superfluid helium, the photo-luminescence excitation spectrum of single Pr^{3+} ion was measured in a bulk crystal of LaF$_3$ at 1.5 K. The maximum luminescence intensity, 45 ± 5 cps, is consistent with the estimation of 30 cps from the bulk parameters. The linewidth of the single Pr^{3+} spectrum was 3 MHz. The origin of the broadening is not clear. To investigate the origin in detail, the sensitivity of the setup must be improved, the width observed in the
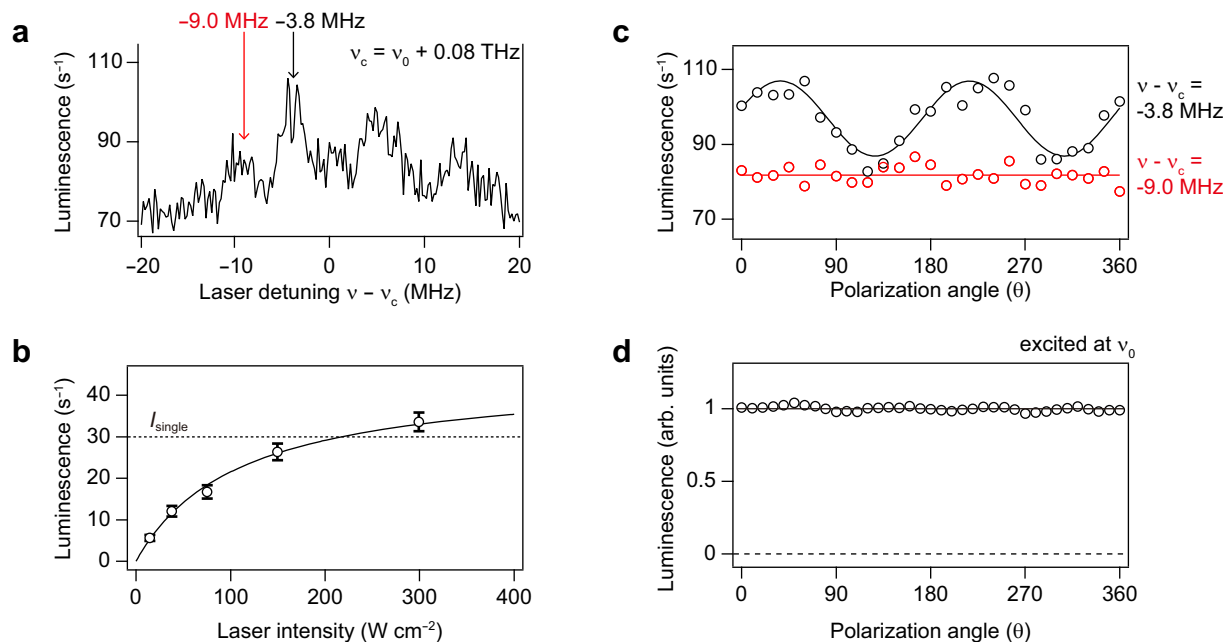
Figure 6 | Saturation behavior and polarization dependence of single Pr^{3+} ion in LaF_3 at 1.5 K. (a) Photo-luminescence excitation spectrum of a single Pr^{3+} ion at $\nu_c = \nu_0 + 0.08$ THz (627.41 THz). The total excitation intensity of the three frequency components was 75 W cm^{-2}. (b) Plot of the luminescence intensity of the peak at -3.8 MHz versus the total excitation intensity (see text for details). The dashed line indicates the signal intensity estimated for single-ion luminescence I_{single}. (c) Plot of the intensity at the peak (excited at -3.8 MHz) and at the wing (excited at -9.0 MHz) versus the polarization angle of the excitation light. The total excitation intensity was 75 W cm^{-2}. The two solid lines indicate sinusoidal fitting of the intensity at the peak and the average luminescence intensity at the wing. (d) Plot of the luminescence intensity of ensemble ions versus polarization angle of the excitation light. The excitation laser was set to ν_0.

bulk crystal is narrower than the FWHM of 14 MHz reported for a Pr^{3+}-doped Y_2SiO_5 nanocrystal[14] and the FWHM of 50 neV (= 12 MHz) reported for a Er^{3+} doped single electron transistor[13]. A narrower linewidth is in general more favorable in application to quantum information processing because the information density per unit frequency can be increased. The scheme of Rare-Earth Quantum Computer[5] requires a narrow linewidth for quantum logical operation which employs the transition frequency modulation driven by the interaction with other ions. When used as a nuclear-spin qubit, an external magnetic field will be applied to induce the Zeeman effect. Because the Zeeman effect is anisotropic, the orientation of the sample must be accurately controlled. Control of orientation is easier for a bulk crystal than for a nanocrystal.

Methods

Excitation light source. The light source consists of a continuous wave (CW) tunable diode laser and a MgO-doped periodically poled $LiNbO_3$ (PPMgO:LN) crystal. The PPLN crystal was converted near the infrared output of the diode laser (956 nm) to blue excitation light (478 nm) by second harmonic generation. To keep the excitation frequency resonant with the absorption of a single Pr^{3+} ion, the width of which at 1.5 K is several kHz, the fundamental diode-laser frequency was locked to a temperature-stabilized Fabry-Perot cavity using the Pound-Drever-Hall method[30]. The hole-burning measurement of Pr^{3+}:LaF_3 revealed that the frequency-stabilized SHG light had a FWHM linewidth of 0.4 MHz.

When measuring the photo-luminescence excitation spectrum, two AOMs were used as frequency shifters of the frequency-stabilized output of the PPLN-doubled laser. One AOM produced a 40-MHz scan of the fundamental laser frequency. The other AOM was used as a laser-frequency multiplexer. The laser-frequency shift given by the multiplexer cycles had three values, 0, 16.7 or 8.5, and 25.2 MHz. The cycling period was set to 30 μs. Because the cycling period is shorter than the lifetime of the $^3P_0$ state (47 μs)[26], for the ions in the excited states, a laser of rapidly cycling frequency can be regarded as light that has three frequency components.

Aspheric reflective objective. The aspheric reflecting objective consisted of aspherical convex and spherical concave mirrors (see Fig. 1). The solid angle of collection is expressed as $\Omega = 2\pi(\cos(\theta_{min}) - \cos(\theta_{max}))$, where θ_{max} is half of the angular aperture of the spherical concave mirror and θ_{min} is the minimum angle at which rays are not blocked by the aspherical convex mirror. The relationship between NA and θ_{max} is NA = $n_{He} \sin(\theta_{max})$. θ_{max} of the aspheric reflecting

objective is 74.8°, and θ_{min} is 32.9°. The design value of Ω is 1.16π. When rays were refracted by the interface between LaF_3 and superfluid helium (the ratio of the two refractive indices is $n_{LaF3}/n_{He} = 1.56$)[20,31], θ_{max} and θ_{min} decreased to 38.2° and 20.3°, respectively. Ω became 0.30π (7.6% of all solid angle 4π) for the Pr^{3+} ions doped in LaF_3.

The performance of the aspheric reflective objective (NA = 0.99) was evaluated at 1.5 K from fluorescence images of five single quantum dots (Qdot 705 ITK Carboxyl, Invitrogen) acquired by 3D sample scanning of our confocal setup. With excitation at 532 nm, the fluorescing spot had widths in the focal plane of $\Gamma_{x,y} = 0.212 \pm 0.008$ μm and that along the optical axis of $\Gamma_z = 0.91 \pm 0.04$ μm in in the 1/e^2 full width. $\Gamma_{x,y}$ was very close to the theoretical calculation (0.203 μm), and Γ_z was 1.4 times larger than that of z (0.64 μm). The imperfection of Γ_z was not related to temperature cycling but to manufacturing errors.

Luminescence detection by homemade reflecting confocal microscope. The 0.05% doped Pr^{3+}:LaF_3 bulk crystal was placed in a 1.5 K cryostat together with the reflecting objective. The excitation light was introduced to the microscope via a single-mode fiber and focused on the surface of the sample using the reflecting objective. The red-shifted emission was collected by the same objective, separated from the blue light by a long-wavelength-pass filter and coupled to a multi-mode fiber. The fiber ends served as the excitation and the detection pinholes of the confocal microscope. The number of signal photons passing through the fiber was counted by the SPCM. The optical transmittance of the entire microscope was 11%, which included reflection and transmission losses from all components from the reflective objective to the multi-mode fiber. The quantum efficiency of the SPCM is 0.58. As discussed above, the solid angle of the objective is 7.6% of the entire solid angle. The detection efficiency of emission from a single Pr^{3+} ion in a LaF_3 crystal estimated using these values was 0.43%.

1. Neumann, P. *et al.* Single-shot readout of a single nuclear spin. *Science* **329**, 542–544 (2010).
2. Robledo, L. *et al.* High-fidelity projective read-out of a solid-state spin quantum register. *Nature* **477**, 574–8 (2011).
3. Houel, J. *et al.* High Resolution Coherent Population Trapping on a Single Hole Spin in a Semiconductor Quantum Dot. *Phys. Rev. Lett.* **112**, 107401 (2014).
4. Sleiter, D. J. *et al.* Optical pumping of a single electron spin bound to a fluorine donor in a ZnSe nanostructure. *Nano Lett.* **13**, 116–120 (2013).
5. Ohlsson, N., Krishna Mohan, R. & Kröll, S. Quantum computer hardware based on rare-earth-ion-doped inorganic crystals. *Opt. Commun.* **201**, 71–77 (2002).
6. Macfarlane, R. Inhomogeneous broadening of spectral lines in doped insulators. *J. Lumin.* **45**, 5004–5011 (1990).

7. Rippe, L., Nilsson, M., Kröll, S., Klieber, R. & Suter, D. Experimental demonstration of efficient and selective population transfer and qubit distillation in a rare-earth-metal-ion-doped crystal. *Phys. Rev. A* **71**, 062328 (2005).

8. Goto, H. & Ichimura, K. Observation of coherent population transfer in a four-level tripod system with a rare-earth-metal-ion-doped crystal. *Phys. Rev. A* **75**, 033404 (2007).

9. Klein, J., Beil, F. & Halfmann, T. Robust Population Transfer by Stimulated Raman Adiabatic Passage in a Pr^{3+}:Y_2SiO_5 Crystal. *Phys. Rev. Lett.* **99**, 113003 (2007).

10. Rodrigues-Herzog, R. *et al.* Optical microscopy of single ions and morphological inhomogeneities in Sm-doped CaF2 thin films. *Phys. Rev. B* **62**, 11163–11169 (2000).

11. Bartko, A. P. *et al.* Observation of dipolar emission patterns from isolated Eu^{3+}:Y_2O_3 doped nanocrystals: new evidence for single ion luminescence. *Chem. Phys. Lett.* **358**, 459–465 (2002).

12. Malyukin, Y. V., Masalov, A. A. & Zhmurin, P. N. Single-ion fluorescence spectroscopy of a Y_2SiO_5:Pr^{3+} nanocluster. *Phys. Lett. A* **316**, 147–152 (2003).

13. Yin, C., Rancic, M., Boo, G. de & Stavrias, N. Optical addressing of an individual erbium ion in silicon. *Nature* **497**, 91–94 (2013).

14. Utikal, T. *et al.* Spectroscopic detection and state preparation of a single praseodymium ion in a crystal. *Nat. Commun.* **5**, 3627 (2014).

15. Siyushev, P. *et al.* Coherent properties of single rare-earth spin qubits. *Nat. Commun.* **5**, 3895 (2014).

16. Kolesov, R. *et al.* Optical detection of a single rare-earth ion in a crystal. *Nat. Commun.* **3**, 1029 (2012).

17. Hinohara, T., Hamada, Y. I., Nakamura, I., Matsushita, M. & Fujiyoshi, S. Mechanical stability of a microscope setup working at a few kelvins for single-molecule localization. *Chem. Phys.* **419**, 246–249 (2013).

18. Fujiwara, M., Fujiyoshi, S. & Matsushita, M. Single-component reflecting objective for ultraviolet imaging and spectroscopy at cryogenic temperature. *J. Opt. Soc. Am. B* **26**, 1395–1399 (2009).

19. Fujiwara, M., Fujiyoshi, S. & Matsushita, M. Single-component reflecting objective for low-temperature imaging and spectroscopy of single nano objects. *Phys. Procedia* **13**, 38–41 (2011).

20. Burton, E. F. Refractive Indexes of Helium I and II. *Nature* **140**, 1015–1015 (1937).

21. Wong, E. Y., Stafsudd, O. M. & Johnston, D. R. Absorption and Fluorescence Spectra of Several Praseodymium-Doped Crystals and the Change of Covalence in the Chemical Bonds of the Praseodymium Ion. *J. Chem. Phys.* **39**, 786–793 (1963).

22. Chen, Y. C., Chiang, K. & Hartmann, S. R. Spectroscopic and relaxation character of the $^3P_0$-$^3H_4$ transition in LaF_3:Pr^{3+} measured by photon echoes. *Phys. Rev. B* **21**, 40–47 (1980).

23. Erickson, L. E. The nuclear quadrupole interaction in Pr^{3+}:LaF_3 — An optical-RF double resonance measurement of the ground electronic state. *Opt. Commun.* **21**, 147–149 (1977).

24. Shelby, R., Macfarlane, R. & Yannoni, C. Optical measurement of spin-lattice relaxation of dilute nuclei: LaF_3:Pr^{3+}. *Phys. Rev. B* **21**, 5004–5011 (1980).

25. Moerner, W. E. & Kador, L. Optical detection and spectroscopy of single molecules in a solid. *Phys. Rev. Lett.* **62**, 2535–2538 (1989).

26. Brown, M. R., Whiting, J. S. S. & Shand, W. A. Ion—Ion Interactions in Rare-Earth-Doped LaF_3. *J. Chem. Phys.* **43**, 1–9 (1965).

27. Weber, M. J. Spontaneous Emission Probabilities and Quantum Efficiencies for Excited States of Pr^{3+} in LaF_3. *J. Chem. Phys.* **48**, 4774–4780 (1968).

28. Macfarlane, R. M. & Shelby, R. M. *Spectroscopy of solids containing rare-earth ion* (North-Holland, Amsterdam, 1987).

29. Lee, K. G. *et al.* A planar dielectric antenna for directional single-photon emission and near-unity collection efficiency. *Nat. Photonics* **5**, 166–169 (2011).

30. Drever, R. W. P. *et al.* Laser phase and frequency stabilization using an optical resonator. *Appl. Phys. B Photophysics Laser Chem.* **31**, 97–105 (1983).

31. Laiho, R. & Lakkisto, M. Investigation of the refractive indices of LaF_3, CeF_3, PrF_3 and NdF_3. *Philos. Mag. Part B* **48**, 203–207 (1983).

Acknowledgments

Author contributions

The experiment was conceived by S.F. and M.M. and performed by I.N. H.I. and S.F. designed the new reflecting objective. I.N. and T.Y. constructed the experimental setup. I.N., S.F. and M.M. discussed the results and wrote the manuscript.

Additional information

How to cite this article: Nakamura, I., Yoshihiro, T., Inagawa, H., Fujiyoshi, S. & Matsushita, M. Spectroscopy of single Pr^{3+} ion in LaF_3 crystal at 1.5 K. *Sci. Rep.* **4**, 7364; DOI:10.1038/srep07364 (2014).